Translational Oncology
www.transonc.com

Volume 12 Number 9 September 2019 pp. 1196–1205 1196

Tumor Site-Dependent Transport Properties Determine Nanotherapeutics Delivery and Its Efficacy

Megumi Kai, Arturas Ziemys, Yan ting Liu, Milos Kojic, Mauro Ferrari and Kenji Yokoi

Department of Nanomedicine, Houston Methodist Research Institute, 6670 Bertner Street, Houston, TX 77030, USA

Abstract

Insufficient delivery of systemically administered anticancer drugs to tumors can compromise therapeutic efficacy and develop drug delivery-based therapeutic resistance. Nanotherapeutics such as PEGylated liposomal doxorubicin (PLD) are designed to preferentially accumulate in tumors utilizing enhanced permeation and retention effect. However, their antitumor effects and resulting clinical outcomes are modest and heterogeneous among tumors. Here, we aimed to investigate whether the amount and efficacy of PLD delivered to tumors are tumor site dependent. We established orthotopic primary tumor or liver metastases models of murine breast cancer using 4 T1 cells. PLD showed significant therapeutic effects against tumors that grew in primary mammary sites but not in the liver. We found that differences in therapeutic efficacy were not because of the intrinsic biological resistance of cancer cells but rather were associated with tumor site-dependent differences in transport properties, such as the amount of PLD delivery, blood vessel function, relative vascular permeability, and mechanical pressure in tumors. Thus, transport properties in tumor is site dependent and can be used as phenotypic surrogate markers for tumor drug delivery and therapeutic efficacy.

Translational Oncology (2019) 12, 1196–1205

Introduction

Heterogeneous responses of tumors located in different sites to systemically administered anticancer therapeutics have long been recognized in the clinic. However, little is known about the exact mechanisms for such site-specific heterogeneity [1,2]. Resistance mechanisms based on the levels of genetic, epigenetic, and transcription factor in cancer cells have been explored [3–5]. As a result of cross-talk between cancer cells and the host microenvironment, the development and function of tumor-associated blood vessels and the extracellular matrix can also be affected by cancer cells, which in turn influence the various transport properties within the tumors [6,7]. The heterogeneity of these transport properties in tumors can hinder drug delivery and affects therapeutic efficacy [6,8–10]. Insufficient drug delivery to tumors below the threshold concentration that can induce cytotoxic effects on cancer cells generates "transport-based therapeutic resistance," even for agents with proven efficacy against cancer cell lines in vitro [11,12].

Nanotherapeutics, such as pegylated liposomal doxorubicin (PLD), are high-payload delivery vehicles with extensive systemic pharmacokinetic profiles and enhance drug delivery within tumors utilizing the enhanced permeation and retention effect [13]. Nevertheless, the therapeutic efficacy of PLD is heterogeneous and has not shown significantly improved antitumor effects over conventional chemotherapeutics in patients with metastatic breast cancer [14,15]. Such clinical evidence suggests that PLD delivery to metastatic breast tumors is insufficient and variable. Therefore, to improve therapeutic efficacy, it is important to determine transport properties in tumors to elucidate the mechanisms responsible for the heterogeneity of tumor responses to PLD.

We have previously shown the tumor type dependent difference in transport properties in subcutaneous tumors, the amount of PLD delivery and the therapeutic efficacy using syngeneic mouse tumor models of breast and lung cancers [16]. In this study, we found tumor site-dependent differences in PLD efficacy in syngeneic mouse

Address all correspondence to: Mauro Ferrari or Kenji Yokoi, Department of Nanomedicine, Houston Methodist Research Institute, 6670 Bertner Street, R7-118, Houston, TX 77030, USA. E-mail: mauroferrari.outsidehmh@gmail.com
Received 22 February 2019; Revised 11 May 2019; Accepted 13 May 2019

1936-5233/19
https://doi.org/10.1016/j.tranon.2019.05.011

primary tumor and liver metastatic models of breast cancer. We found that the differences can be attributed to transport properties and PLD delivery in each tumor site. Thus, transport properties in tumor are site dependent and can act as phenotypic surrogates of therapeutic responses.

Material and Methods

Cell Culture

The 4 T1 murine breast cancer cell line was obtained from and characterized by ATCC (Manassas, VA). The cells were cultured in complete minimal essential medium supplemented with 10% fetal bovine serum (Life Technologies, Inc., Grand Island, NY) and a penicillin–streptomycin cocktail (Flow Laboratories, Rockville, MD).

Mice

Female BALB/c mice, 5–7 weeks of age, were purchased from Charles River Laboratories (Wilmington, MA). The mice were maintained in animal facilities at the Houston Methodist Research Institute approved by the American Association for Accreditation of Laboratory Animals.

Establishment of Primary Tumor and Experimental Liver Metastases

To establish primary tumor, 1×10^5 4 T1 cells in 100 μL phosphate-buffered saline (PBS) were injected into mouse mammary fat pad (mfp). To establish experimental liver metastases in another set of mice, 4 T1 cells (1×10^5/100 μL) were injected into spleen body followed by splenectomy. The cells injected into spleen disseminate to the liver through the portal vein [17,18]. All protocols were approved by the Institutional Animal Care and Use Committee of the Houston Methodist Research Institute.

Therapy and Necropsy

Nine days after the inoculation of tumor cells, mice bearing primary tumor or liver metastases were randomized to receive an intravenous (i.v.) injection of PBS (n = 5) or 8 mg/kg PLD (Doxoves™-Liposomal Doxorubicin HCl; FormuMax Scientific Inc., Palo Alto, CA) (n = 5). Then, tumor-bearing mice were sacrificed 6 days after therapy. Primary tumors or livers were excised, frozen, and stored at −80 °C for subsequent analyses. The therapeutic efficacy of PLD against tumor growth was evaluated using the following methods: (1) primary tumor size was measured, and tumor volume (V) was calculated using the formula, V = 1/2(length × width^2), and (2) the size of liver metastases was estimated from two-dimensional tumor measurements (the product of the longest diameter and its longest perpendicular diameter for each tumor) on a captured immunofluorescence image using ImageJ software (NIH, Bethesda, MD) [19].

Imaging Perfused Blood Vessels in Tissues by Fluorescently Labeled Tomato Lectin

An intravascular injection of tomato lectin leads to labeling of functional blood vessels [20]. In another set of tumor-bearing mice (Day15, n = 5/tumor site), DyLight 488-labeled tomato lectin (DL1174) (Vector Laboratories, Inc., Burlingame, CA) was injected i.v. (100 μg/100 μL). Five minutes after the injection, incision of the inferior vena cava was made, 10 mL PBS and 10 mL of 4% paraformaldehyde were injected via the left ventricle, and tumors were harvested.

Immunofluorescence Imaging of Tumor Cell Proliferation, Apoptosis

Frozen sections were fixed in 4% paraformaldehyde in PBS. For Ki67 staining to image cell proliferation, the sections were blocked with blocking solution (0.3% Triton X, 5% horse sera, and 1% goat sera in PBS). Anti-Ki67 antibody (ab15580) (Abcam, Cambridge, MA) was applied to the blocking solution followed by the addition of Alexa Fluor® 488 anti-rabbit IgG (Jackson ImmunoResearch, West Grove, PA). To evaluate cell apoptosis, a TUNEL assay was performed, according to the manufacturer's protocol (Promega Corporation, Madison, WI). All images were acquired using a Nikon A1 microscope (Nikon Inc., Melville, NY).

PLD Delivery to Primary Tumors and Liver Metastases

Mice bearing primary tumors or liver metastases were i.v. injected with PLD as described above (n = 5/each site) to evaluate PLD delivery to tumors. Previously, we performed PLD kinetics analysis in 4 T1 tumor and found the t max was 24 hours after the i.v. injection [21]. In the current study, we sacrificed mice 24 hours after the injection and primary tumors or livers were harvested for immunofluorescence imaging. Frozen sections were stained with DAPI and PLD accumulation into the tumor was evaluated using wide-field imaging system [ImageXpress Micro, (Molecular Devices, LLC, San Jose, CA)] by imaging the ruby red fluorescence of doxorubicin (DOX) at the excitation and emission wavelengths of 488 nm and 590 nm, respectively.

Free DOX Delivery to Liver Metastases

Mice bearing liver metastases were also i.v. injected with free DOX (8 mg/kg) and sacrificed at 3 min, 3 hour, or 24 hours (n = 5/each) for fluorescence imaging of doxorubicin inside liver metastases and uninvolved liver as described above.

Primary Tumor Cell Cultures

Fresh tumor tissues were aseptically harvested from primary tumors or liver metastases. Using autoclaved instruments, the tissues were minced into small pieces and homogenized. Cell suspensions were centrifuged at 300 x *g* for 3 minutes three times, filtered through a 40-μm cell strainer (BD Biosciences, San Jose, CA), seeded onto 6-well culture plates, and incubated for 1–2 days. Cells were passaged into larger flasks when 70–80% confluence was reached [22]. Primary cell cultures were established within 2 weeks.

Cell Toxicity and Viability Assay (MTT Assay)

One thousand cells from the established primary culture were seeded into a 96-well plate and incubated with different concentrations of PLD (0–200 μg/mL) for 3 days. Then, 20 μL of an MTT {[3-(4, 5- dimethylthiazol-2yl)-2,5-diphenyltetrazolium bromide] (Sigma, St. Louis, MO)} solution were added to each well, and the absorbance was recorded at an optical density of 560 nm after subtracting the background absorbance at 670 nm [23].

Statistical Analysis

Results are expressed as the mean ± SD, and differences between groups were assessed by the Mann–Whitney test using GraphPad Prism software, version 6.05 (GraphPad Software, San Diego, CA). *P* values less than 0.05 were considered statistically significant.

Results

Primary Breast Tumors, But Not Liver Metastases, Responded to Systemically Administered PLD

To evaluate the therapeutic efficacy of PLD against tumors growing in different sites, we established primary tumor-bearing mice and experimental liver metastases–bearing mice using 4 T1 cells. Both types of tumor-bearing mice were then randomized for an i.v. injection of either vehicle control (PBS) or PLD (8 mg/kg). All mice were sacrificed 6 days after therapy, and the therapeutic efficacy of PLD against tumor growth was evaluated. Although PLD significantly inhibited primary tumor growth compared to control therapy, liver metastases did not show any significant responses to PLD (Figure 1, *A* and *B*). This finding suggests that PLD antitumor efficacy depends on the tumor site.

PLD Reduced Cell Proliferation and Increased Apoptosis in Primary Tumors But Not in Liver Metastases

Next, we determined tumor site-dependent differences in tumor pharmacodynamics in response to PLD. We performed immunohistochemical analyses of tissue sections using proliferation maker Ki67, and apoptosis assays using a TUNEL kit. Tumor cell proliferation was significantly decreased by PLD therapy compared to controls in primary tumors but not in liver metastases (Figure 2, *A* and *C*). The number of apoptotic cells was significantly increased in primary tumors but not in liver metastases after PLD treatment compared to control therapy (Figure 2, *B* and *D*). These findings suggest that tumor pharmacodynamics are tumor site dependent.

The Amount of PLD Delivered to the Tumor Was Site Dependent

We have previously shown that cancer type-dependent differences in PLD delivery to subcutaneous tumors are associated with therapeutic efficacy and transport properties of tumors. In this study, we hypothesized that the site-dependent differences in the pharmacodynamics of tumors can be attributed to PLD delivery and transport properties in tumors. To test our hypothesis, we evaluated PLD delivery to primary tumors and liver metastases by imaging the intrinsic fluorescence of doxorubicin using a wide-field imaging system and confocal microscopy. In primary tumors, doxorubicin was primarily delivered to the periphery rather than to the inside of the tumors (Figure 3*A*). In contrast, we found that doxorubicin accumulated primarily outside of the tumors, with little accumulating inside liver metastases (Figure 3*B*). This finding is consistent with that in our previous study in which i.v.-injected PLD was primarily engulfed by Kupffer cells in the liver [10]. More highly magnified images also confirmed this trend; a significantly lower quantity of doxorubicin accumulated in individual liver metastases compared to primary tumors (Figure 3*C*, and *D*). Taken together, the delivery of PLD to 4 T1 tumors significantly differed between tumor sites. We also evaluated kinetics of free DOX in the liver metastases which increased and rapidly diminished within 24 hours. The area under the curve of DOX inside tumor was much less than that in uninvolved liver sinusoids (Supplementary material).

The Number of Perfused Blood Vessels Was More Abundant in Primary Tumors Than in Liver Metastases

To determine the different mechanisms involved in PLD delivery between primary tumors and liver metastases, we evaluated the functions of tumor-associated blood vessels. We imaged perfused blood vessels by the i.v. injection of fluorescently labeled tomato lectin, which binds to surfaces of endothelial cells only in perfused blood vessels. As shown in Figure 4*A*, i.v.-injected tomato lectin was able to label vessels inside primary tumors. This dense pattern of vascular labeling was present throughout the tumor, especially at the periphery. In contrast, only a few lectin-labeled blood vessels were found inside liver metastases (Figure 4*B*). Instead, numerous sinusoids in the surrounding liver were densely labeled with lectin. The amount of tomato lectin in primary tumors was significantly higher than in liver metastases. These results suggest that the number of perfused blood vessels in tumors are responsible for differences in PLD delivery.

The Levels of Type IV Collagen and Cell Density Were Higher in Liver Metastases Than in Primary Tumors

To determine the mechanisms responsible for tumor site-dependent differences in the levels of perfused tumor-associated blood vessels, we investigated various transport properties in tumors. First, we performed immunohistochemical staining of tumor tissues using an antibody to CD31 to image both perfused and non-perfused blood vessels. It is surprising to note that more blood vessels developed in liver metastases than in primary tumors (Figure 5, *A* and *B*). This result indicates that more tumor-associated blood vessels

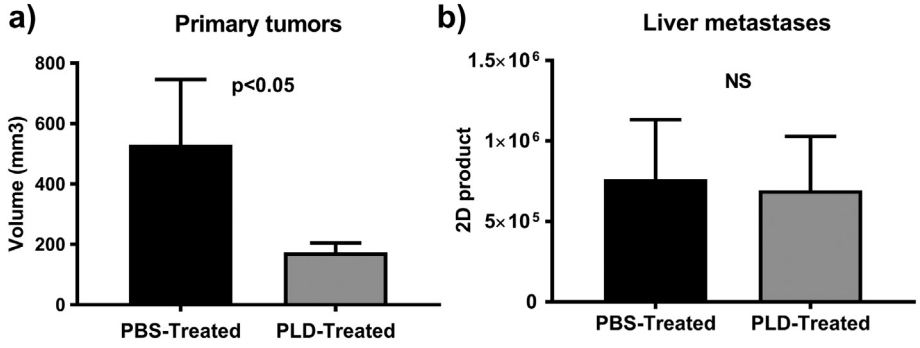

Figure 1. Tumor site-dependent differences in the therapeutic efficacy of PLD against tumor growth. Nine days after 4 T1 cells were inoculated into the mfp or spleen, tumor-bearing mice were treated with control PBS or PLD, respectively. Six days after treatment, therapeutic efficacy was evaluated in (a) primary tumors and (b) liver metastases (b). Y-axis in (a) shows tumor volume (mm^3), y-axis in (b) shows two-dimensional (2D) tumor measurements (the product of the longest diameter and longest perpendicular diameter for each tumor). NS: not significant.

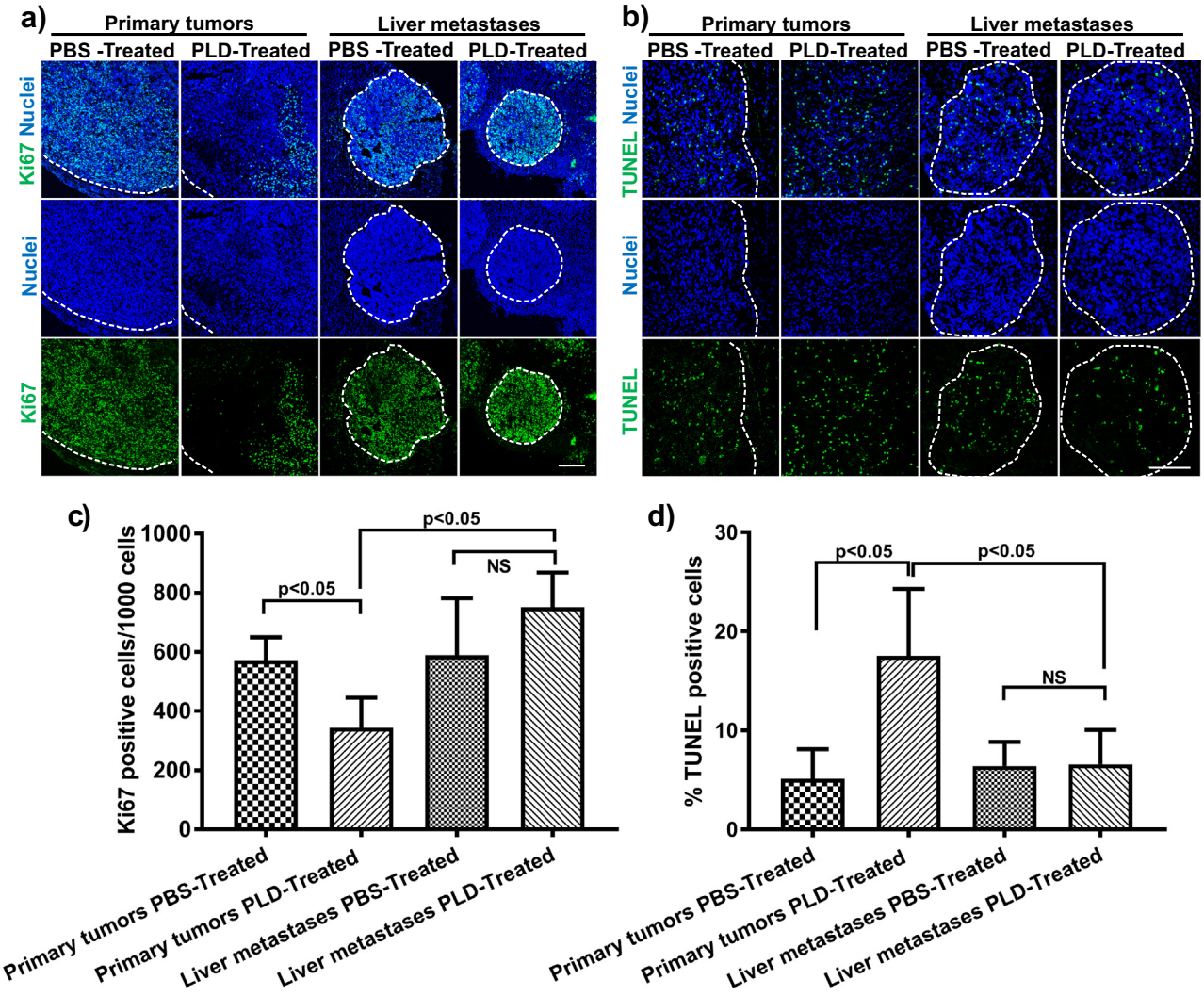

Figure 2. Analysis of tumor cell proliferation and apoptosis after PLD treatment. (a) Immunofluorescence of Ki67, a tumor cell proliferation marker, and (b) analysis of apoptosis using the TUNEL assay in primary tumors and liver metastases are shown. Quantification of the imaging data shown in primary tumors (c) and liver metastases (d). NS: not significant. Scale bar, 200 μm.

develop inside liver metastases, but their extent of perfusion is compromised to a greater extent than that in primary tumors.

Next, we imaged the amount and location of type IV collagen, known to be a major constituent of the basal membrane surrounding blood vessels and the extracellular matrix. Type IV collagen in tumors provides structural support to the tissue matrix, influences interstitial pressure, and plays a critical role in blood vessel functions [24]. We previously reported an inverse correlation between the amount of type IV collagen in the basal membrane, which co-localizes with endothelial cells, and the vascular permeability of blood vessels to PLD [16]. In this study, the total amount of type IV collagen was significantly higher inside liver metastases than in primary tumors. The co-localization of type IV collagen with endothelial cells was also higher in liver metastases. These data indicate that while relative interstitial pressure can be higher, vascular permeability can be lower in liver metastases compared to primary tumors.

It has been reported that cancer cells inside tumors can cause tumor-associated blood vessels to become mechanically compressed and collapsed [25]. We compared site-dependent differences in the tumor's mechanical microenvironment by imaging cell density. As shown in Figure 5, *D* and *E*, liver metastases had a significantly higher density of constituent cells (median cell count 13,476/mm^2) compared to that in primary tumors (8236/mm^2) and uninvolved liver sinusoid area (2238/mm^2), indicating that a significantly reduced amount of extracellular space exists in liver metastases, including space for the vasculature. Taken together, both the higher density of cells and the amount of extracellular matrix protein in liver metastases can compress and collapse blood vessels and increase the level of resistance of blood perfusion more significantly than in primary tumors.

The Intrinsic Resistance Properties of 4 T1 Cells to Doxorubicin Were Not Responsible for Tumor Site-Dependent Differences in PLD Therapeutic Efficacy

The intrinsic resistance of cancer cells to PLD, independent of factors derived from drug delivery, can be fundamental for determinations of therapeutic efficacy. To determine the differences in the intrinsic drug resistance of cancer cells growing in primary sites versus as liver metastases, we established primary cell cultures from both sites in mice treated with or without PLD. These cell lines were incubated with PLD in vitro, and cell proliferation was evaluated

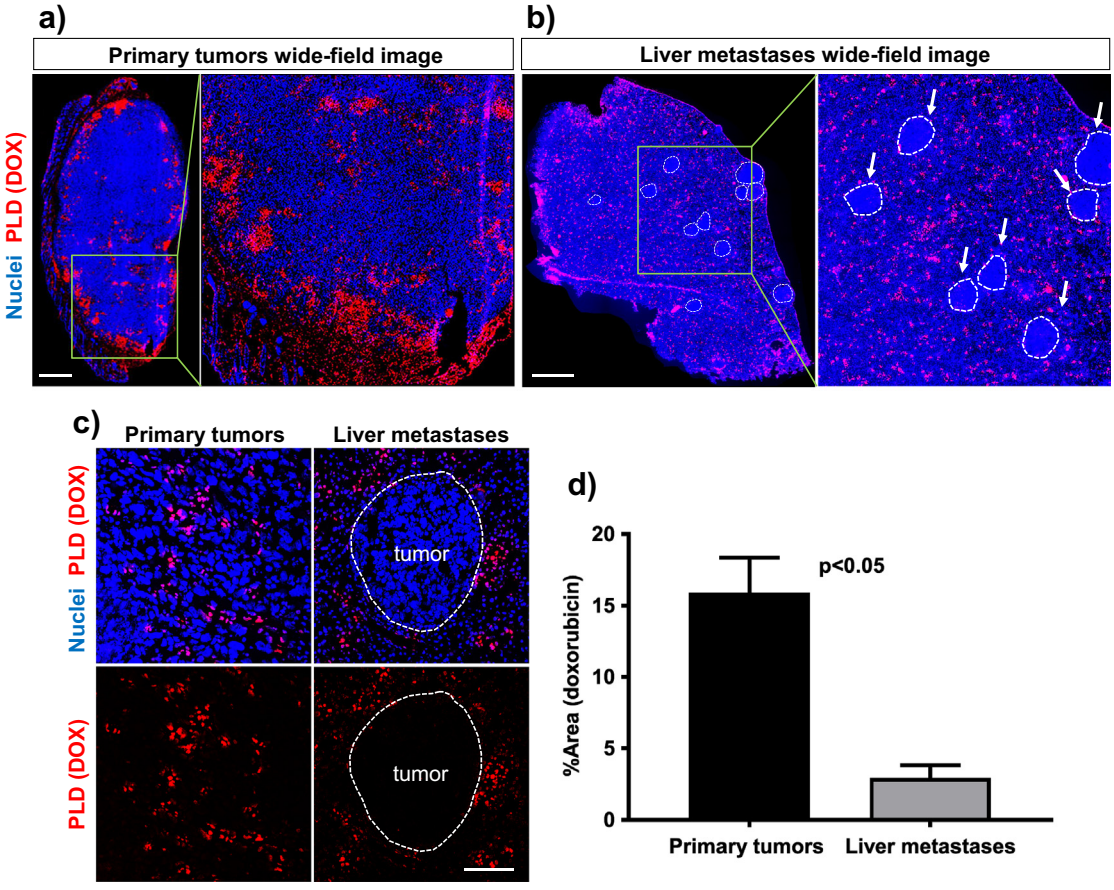

Figure 3. PLD delivery to primary tumors and liver metastases. Fluorescence of DOX delivered to primary tumors and liver metastases was analyzed using a wide-field imaging system (a and b) and confocal microscopy (c). Arrows indicate individual liver metastasis. (d) Quantification of the imaging data. Scale bar, 1 mm in (a and b), 100 μm in (c) respectively. DOX, doxorubicin.

using an MTT assay. Interestingly, 4 T1 cells established from liver metastases showed slightly higher sensitivity to PLD compared to cells that originated from primary tumors in PLD therapy-naïve mice (Figure 6*A*). No significant differences in the PLD sensitivity of cells established from primary tumors and liver metastases of mice treated with PLD were found (Figure 6*B*).

P-glycoprotein is associated with efflux pumps expressed on the cell membrane; these pumps are responsible for decreased drug

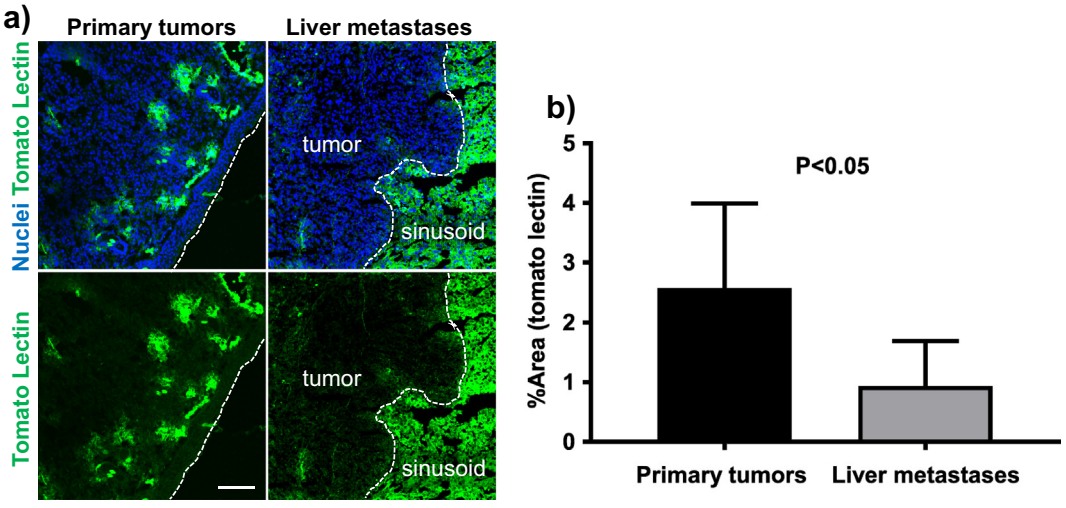

Figure 4. Imaging the perfusion of tumor-associated blood vessels by i.v. injection of fluorescently labeled tomato lectin. (a) Labeling of blood vessels in primary tumors and liver metastases. Nuclei were stained with DAPI (shown in blue) Scale bar, 100 μm. (b) Quantification of the amount of tomato lectin shown in (a) and expressed as % area using ImageJ software.

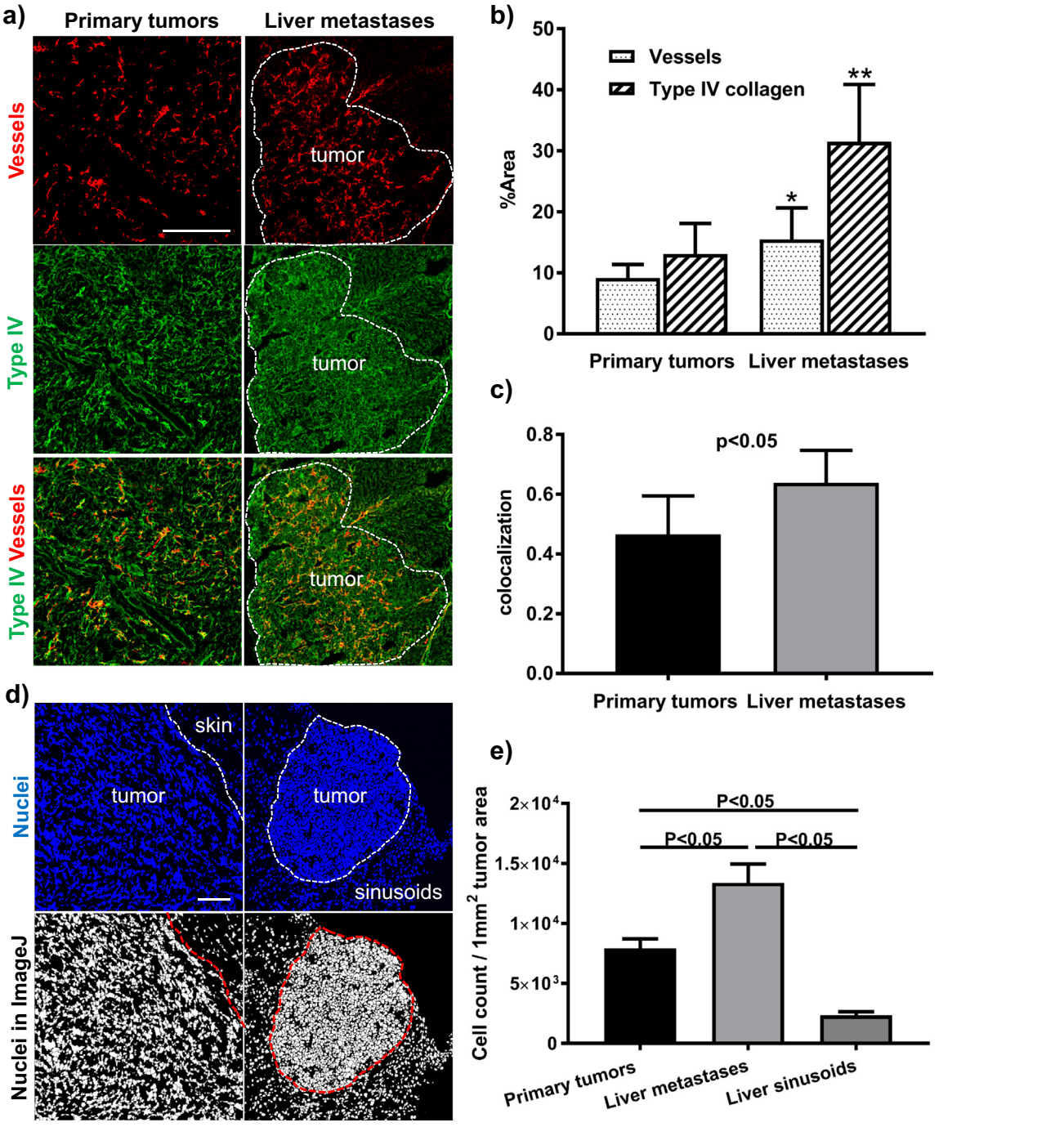

Figure 5. Imaging of drug transport-related molecules in primary tumors and liver metastases. (a) Immunofluorescence imaging of tumor tissues using antibodies to CD31 and type IV collagen. Scale bar, 200 μm. (b) Quantification of the labeling shown in (a) and expressed as % area (* indicates $P < .05$ with respect to vessels between primary tumors and liver metastases; ** indicates $P < .05$ with respect to type IV collagen between primary tumors and liver metastases). (c) Quantification of the labeling overlay shown in (a). (d) Imaging of cell density by immunofluorescence imaging of nuclei (DAPI) in primary tumors, liver metastases and uninvolved liver sinusoids (upper panel). Scale bar, 100 μm. Images were converted to black and white, and quantified using ImageJ software (lower panel). (e) Quantification of the DAPI labeling.

accumulation in multidrug-resistant cells. An immunohistochemical analysis using a p-glycoprotein antibody showed no significant differences in its expression levels between the two tumor sites.

Together, the intrinsic resistance mechanism of 4 T1 cells derived from primary tumors or liver metastases is unlikely the cause of the differential responses to PLD. Therefore, the sensitivity of a tumor to PLD in vivo can be determined by the amount of PLD delivered to the tumor, which depends on the drug transport properties of the tumor, such as the perfusion and permeability of tumor-associated blood vessels, as well as the mechanical and interstitial pressures.

Discussion

Our goal was to understand the roles that tumor site-dependent transport properties and drug delivery play in PLD therapeutic

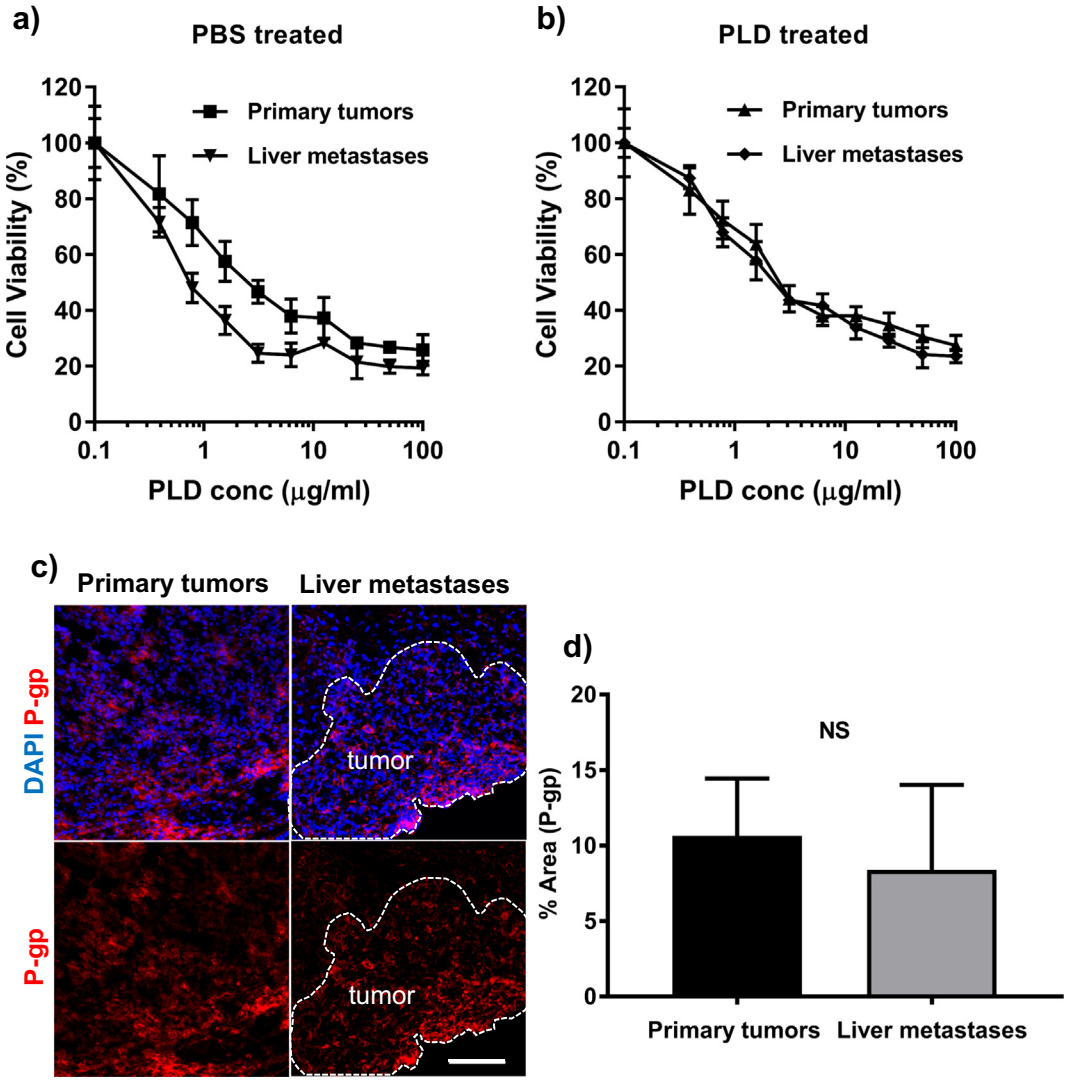

Figure 6. Evaluation of intrinsic drug-resistance properties of 4 T1 cells to doxorubicin. Cell viability after PLD treatment of cell cultures established from primary tumors and liver metastases in PLD therapy-naïve mice (a) and PLD-treated mice (b). (c) Immunofluorescence of p-glycoprotein expression in primary tumors and liver metastases. Scale bar, 100 μm. (d) Quantification of the labeling shown in (c). P-gp: P-glycoprotein, NS: not significant.

efficacy. First, we took a pharmacodynamics approach to identify the effects of PLD on tumor cell proliferation and apoptosis. This approach was used to selectively detect tumor cells into which sufficient concentrations of PLD were delivered to induce cytotoxicity [26]. To determine the reason behind the differences in pharmacodynamics, we evaluated PLD delivery to the tumors by imaging immunofluorescence of anthracyclines. We identified significant differences in the levels of doxorubicin delivered to tumors at different sites. These data suggest that current research must take tumor sites into account when developing novel therapeutics and testing therapeutic efficacy in in vivo tumor models.

In our previous study, PLD accumulation was evaluated in the mice-bearing brain metastases of 4 T1 [16]. Interestingly, 4 T1 tumors in the brain were accumulated with PLD and the survival of the tumor-bearing mice was significantly extended by i.v. injection of PLD. We also found consistent unresponsiveness of 4 T1 liver metastases to PLD [10]. In this study, mean liver metastases size increased from 250 μm to 500 μm in 4 days regardless of systemic therapy with PLD or control PBS. Furthermore, we evaluated delivery and therapeutic efficacy of PLD using another tumor type, 3LL, murine lung cancer growing in the brain or subcutaneously. 3LL tumors was not accumulated with PLD regardless of tumor location and PLD therapy failed to extend survival of 3LL tumor-bearing mice. Dumont et al. reported in the preclinical study that while PLD showed significant anti-tumor effect on primary tumor models, it failed to inhibit development of lung metastasis [27]. Lee et al. reported that higher accumulation of ^{64}Cu labeled liposome into various mouse tumor models was associated with significantly greater anti-tumor activity after treatments with different liposomal drugs [28]. In clinical study, Lee et al. reported that higher tumor deposition of ^{64}Cu labeled liposomal doxorubicin was associated with more favorable treatment outcome of patients with metastatic breast cancer [29]. These data suggest that the nanoparticle imaging approach in clinic can be developed to build biomarker strategy for personalizing nanoparticle-based therapeutics.

The delivery of systemically administered nanotherapeutics to tumors can be constrained by various biophysical barriers, among which tumor-associated blood vessels are the first fundamental barrier

[30,31]. Abnormal perfusion of tumor-associated blood vessels can directly impact therapeutic delivery [15,32]. We evaluated the number of perfused tumor-associated blood vessels by the i.v. injection of fluorescently labeled tomato lectin [20]. Interestingly, the number of perfused blood vessels was significantly lower in liver metastases compared to primary tumors. To determine the mechanism responsible for the limited perfusion of blood vessels in liver metastases, we evaluated the number of tumor-associated blood vessels that developed in tumors by the immunofluorescent staining of tumor sections. To our surprise, the number of blood vessels was higher in liver metastases compared to primary tumors, indicating that while more tumor-associated blood vessels exist in liver metastases, these vessels were not perfused to the same extent as those in primary tumors. This result indicates that immunostaining of an endothelial cell marker in tissue sections is not sufficient to evaluate the level of blood perfusion in tumors, because staining data include both perfused and non-perfused blood vessels. Thus, functional analyses of blood vessels are needed to estimate the drug transport properties of tumors. It also suggests that anti-angiogenic drug loaded nanoparticles may not be sufficiently delivered to the liver metastases and therapeutic efficacy could be limited.

Next, we elucidated the factors that determine whether tumor-associated vessels are perfused. The role of a tumor's mechanical microenvironment during disease progression and mass transport properties is emerging [33]. Elevated interstitial fluid pressure, a hallmark of solid tumors, is a common cause of intratumoral compression [34,35]. In addition, cancer cells inside tumor mass can cause blood vessels within the tumor to mechanically compress and collapse [25]. We compared the site-dependent differences in tumor's mechanical microenvironment from the aspect of the density of cell compositions. Liver metastases were more densely packed with constituent cells compared to primary tumors, indicating that the extracellular space was more limited than in primary tumors. We also found that the total amount of type IV collagen, one of the most abundant extracellular matrix proteins, that can increase interstitial pressure, was more abundant in liver metastases than in primary tumors. These data indicate that both mechanical and interstitial pressures are higher in liver metastases, can collapse tumor-associated blood vessels, and can reduce levels of blood perfusion in liver metastases more significantly than in primary tumors.

We also estimated the vascular permeability of tumor-associated blood vessels, which is also a major biophysical barrier for drug delivery [36,37]. Drugs that pass through the capillary endothelial cell layer first encounter the basal membrane, in which major constituent is type IV collagen [13,21]. Previously, we described the impact of type IV collagen in the basal membrane, which was evaluated by imaging co-localization of type IV collagen with CD31, on the diffusive PLD transport [16,21]. In the current study, we found that the levels of type IV collagen that co-localized with endothelial cells were higher in liver metastases compared to primary tumors, indicating that blood vessels in liver metastases have reduced permeability. Taken together, the observation that less drug is delivered to liver metastases compared to primary tumors can be attributed to limited blood vessel perfusion, higher mechanical and interstitial pressures, and lower vascular permeability.

We previously reported that free DOX concentrations inside the subcutaneous 4 T1 tumor increased and then rapidly diminished within 24 hours after the i.v. injection which was very similar to that reported by other group [36,38]. In the current study, we also evaluated kinetics of free doxorubicin inside liver metastases as small molecule chemotherapeutics may be less subjective to reduced vascular permeability inside tumors. Nevertheless, kinetics of free DOX in the liver metastases was very similar to that in subcutaneous tumor and the area under the curve of DOX inside tumor was much less than that in uninvolved liver (Supplementary material). These results could be due to the limited vascular perfusion, increased mechanical and interstitial pressures inside liver tumors.

Although we injected the same number of cells into the mfp and spleen, tumor diameters in primary tumors and liver metastases were different, even on the same day after the inoculation of cells. Primary tumors can start growing from clusters of injected cells, whereas liver metastases can begin growing from single to several cells lodge in sinusoids [39,40]. Although it would be optimal to compare the drug transport properties and drug delivery within tumors of a similar size, it would be difficult to establish such tumor models. Because the lifespan of both tumor models was approximately 4 weeks, we assume that the total tumor volume (i.e. tumor stage) was similar between the two models. Instead, we evaluated the relationship between tumor size and PLD accumulation among liver metastases [10]. Imaging analysis revealed that the area fraction of doxorubicin inside tumors was 0–2% when tumor size was <300 μm, while the area fraction was 0–0.5% for larger tumors (diameter 300–1500 μm). This data indicates that larger metastatic tumor could develop transport phenotype with reduced perfusion and diffusion.

While we evaluated transport properties in both tumor sites as key drivers of the differences in PLD delivery and therapeutic resistance, we also evaluated the mechanisms of intrinsic drug resistance of cancer cells in vitro by establishing primary cell cultures from tumor-bearing mice. Interestingly, the sensitivities of these cell cultures from liver metastases and primary tumors to PLD were not obviously different. Unknown factors in this analysis, such as how long the established cultured cells could maintain a cancer cell phenotype in their original tumor microenvironment, could not be fully analyzed. Instead, we tried to evaluate the expression of p-glycoprotein, which is involved in intrinsic drug resistance, in tumor sections. The expression levels of p-glycoprotein in vivo were similar between the tumor sites. These data indicate that site-dependent differences in the responses of tumors to PLD in vivo cannot be explained by differences in the intrinsic drug resistance of cancer cells.

In this study, we used an experimental liver metastasis model that was used to establish a site-specific, rapid, and reproducible development of metastases. Nevertheless, this model only recapitulates later cascade of series of metastatic processes [41,42]. To overcome this disadvantage, the use of a spontaneous metastasis model can be recommended. A spontaneous metastasis model can reproduce all stages of the metastatic cascade and more closely resemble clinical disease [43]. However, variations in the time required to develop metastases, as well as the size and number of tumors, in mice are quite diverse, which can result in the need for a larger number of mice in which to conduct therapeutic studies. Recently, genetically engineered mouse tumor models and patient-derived xenograft models have been developed. However, as in the spontaneous metastasis model, it may take some time to standardize these models regarding the rate of tumor development and optimal time frame for therapy [44].

Conclusions

We identified tumor site-dependent differences in the responses of tumors to PLD in mouse models of murine breast cancer. Although

PLD treatment resulted in a significant reduction in tumor growth compared to control therapy when tumors grew in their primary site, this effect was absent in liver metastases. We showed that the differences in therapeutic efficacy were not due to the intrinsic drug resistance mechanisms of cancer cells but rather to tumor site-dependent differences in transport properties and the amount of PLD delivery. Thus, it is critical to understand the actual levels of transport properties and the amount of drug delivered to patient tumors. The development of both rationally designed drug transport systems and therapeutic strategies based on tumor sites is urgently needed to improve therapeutic efficacy and patient survival.

Supplementary data to this article can be found online at https://doi.org/10.1016/j.tranon.2019.05.011.

Acknowledgements

Funding: This work was supported by the National Cancer Institute (NCI U54CA210181). M. Ferrari would like to acknowledge support via the Ernest Cockrell Jr. Presidential Distinguished Chair.

Declaration of Interest

M. Ferrari is a member of the Board of Directors of Arrowhead Pharmaceuticals. No potential conflicts of interest were disclosed by the other authors.

References

[1] Wright N, Rida PCG, and Aneja R (2017). Tackling intra- and inter-tumor heterogeneity to combat triple negative breast cancer. *Front Biosci (Landmark Ed)* **22**, 1549–1580.

[2] Menzies AM, Haydu LE, Carlino MS, Azer MW, Carr PJ, Kefford RF, and Long GV (2014). Inter- and intra-patient heterogeneity of response and progression to targeted therapy in metastatic melanoma. *PLoS One* **9**e85004.

[3] Burrell RA, McGranahan N, Bartek J, and Swanton C (2013). The causes and consequences of genetic heterogeneity in cancer evolution. *Nature* **501**, 338–345.

[4] Marusyk A, Almendro V, and Polyak K (2012). Intra-tumour heterogeneity: a looking glass for cancer? *Nat Rev Cancer* **12**, 323–334.

[5] Villanueva MT (2012). Cell signalling: Stuck in the middle of chemoresistance and metastasis. *Nat Rev Clin Oncol* **9**, 490.

[6] Chen F, Zhuang X, Lin L, Yu P, Wang Y, Shi Y, Hu G, and Sun Y (2015). New horizons in tumor microenvironment biology: challenges and opportunities. *BMC Med* **13**, 45.

[7] Quail DF and Joyce JA (2013). Microenvironmental regulation of tumor progression and metastasis. *Nat Med* **19**, 1423–1437.

[8] Jain RK (1987). Transport of molecules across tumor vasculature. *Cancer Metastasis Rev* **6**, 559–593.

[9] Koay EJ, Truty MJ, Cristini V, Thomas RM, Chen R, Chatterjee D, Kang Y, Bhosale PR, Tamm EP, and Crane CH, et al (2014). Transport properties of pancreatic cancer describe gemcitabine delivery and response. *J Clin Invest* **124**, 1525–1536.

[10] Ziemys A, Yokoi K, Kai M, Liu YT, Kojic M, Simic V, Milosevic M, Holder A, and Ferrari M (2018). Progression-dependent transport heterogeneity of breast cancer liver metastases as a factor in therapeutic resistance. *J Control Release* **291**, 99–105.

[11] Sanhai WR, Sakamoto JH, Canady R, and Ferrari M (2008). Seven challenges for nanomedicine. *Nat Nanotechnol* **3**, 242–244.

[12] Presant CA, Wolf W, Waluch V, Wiseman C, Kennedy P, Blayney D, and Brechner RR (1994). Association of intratumoral pharmacokinetics of fluorouracil with clinical response. *Lancet* **343**, 1184–1187.

[13] Maeda H, Wu J, Sawa T, Matsumura Y, and Hori K (2000). Tumor vascular permeability and the EPR effect in macromolecular therapeutics: a review. *J Control Release* **65**, 271–284.

[14] Duggan ST and Keating GM (2011). Pegylated liposomal doxorubicin: a review of its use in metastatic breast cancer, ovarian cancer, multiple myeloma and AIDS-related Kaposi's sarcoma. *Drugs* **71**, 2531–2558.

[15] Jain RK and Stylianopoulos T (2010). Delivering nanomedicine to solid tumors. *Nat Rev Clin Oncol* **7**, 653–664.

[16] Yokoi K, Tanei T, Godin B, van de Ven AL, Hanibuchi M, Matsunoki A, Alexander J, and Ferrari M (2014). Serum biomarkers for personalization of nanotherapeutics-based therapy in different tumor and organ microenvironments. *Cancer Lett* **345**, 48–55.

[17] Ozawa S, Shinohara H, Kanayama HO, Bruns CJ, Bucana CD, Ellis LM, Davis DW, and Fidler IJ (2001). Suppression of angiogenesis and therapy of human colon cancer liver metastasis by systemic administration of interferon-alpha. *Neoplasia* **3**, 154–164.

[18] Tanei T, Leonard F, Liu X, Alexander JF, Saito Y, Ferrari M, Godin B, and Yokoi K (2016). Redirecting transport of nanoparticle albumin-bound paclitaxel to macrophages enhances therapeutic efficacy against liver metastases. *Cancer Res* **76**, 429–439.

[19] P. Price, K. Sikora, T. Illidge, Treatment of Cancer Fifth Edition, Taylor & Francis2008.

[20] Robertson RT, Levine ST, Haynes SM, Gutierrez P, Baratta JL, Tan Z, and Longmuir KJ (2015). Use of labeled tomato lectin for imaging vasculature structures. *Histochem Cell Biol* **143**, 225–234.

[21] Yokoi K, Chan D, Kojic M, Milosevic M, Engler D, Matsunami R, Tanei T, Saito Y, Ferrari M, and Ziemys A (2015). Liposomal doxorubicin extravasation controlled by phenotype-specific transport properties of tumor microenvironment and vascular barrier. *J Control Release* **217**, 293–299.

[22] Cheung PF, Yip CW, Ng LW, Lo KW, Wong N, Choy KW, Chow C, Chan KF, Cheung TT, and Poon RT, et al (2014). Establishment and characterization of a novel primary hepatocellular carcinoma cell line with metastatic ability in vivo. *Cancer Cell Int* **14**, 103.

[23] Mosmann T (1983). Rapid colorimetric assay for cellular growth and survival: application to proliferation and cytotoxicity assays. *J Immunol Methods* **65**, 55–63.

[24] Fang M, Yuan J, Peng C, and Li Y (2014). Collagen as a double-edged sword in tumor progression. *Tumour Biol* **35**, 2871–2882.

[25] Padera TP, Stoll BR, Tooredman JB, Capen D, Tomaso Ed, and Jain RK (2004). Cancer cells compress intratumour vessels. *Nature* **427**, 695.

[26] Ernsting MJ, Tang WL, MacCallum NW, and Li SD (2012). Preclinical pharmacokinetic, biodistribution, and anti-cancer efficacy studies of a docetaxel-carboxymethylcellulose nanoparticle in mouse models. *Biomaterials* **33**, 1445–1454.

[27] Dumont N, Merrigan S, Turpin J, Lavoie C, Papavasiliou V, Geretti E, Espelin CW, Luus L, Kamoun WS, and Ghasemi O, et al (2019). Nanoliposome targeting in breast cancer is influenced by the tumor microenvironment. *Nanomedicine* **17**, 71–81.

[28] Lee H, Gaddy D, Ventura M, Bernards N, de Souza R, Kirpotin D, Wickham T, Fitzgerald J, Zheng J, and Hendriks BS (2018). Companion diagnostic (64)Cu-liposome positron emission tomography enables characterization of drug delivery to tumors and predicts response to cancer nanomedicines. *Theranostics* **8**, 2300–2312.

[29] Lee H, Shields AF, Siegel BA, Miller KD, Krop I, Ma CX, LoRusso PM, Munster PN, Campbell K, and Gaddy DF, et al (2017). (64)Cu-MM-302 positron emission tomography quantifies variability of enhanced permeability and retention of nanoparticles in relation to treatment response in patients with metastatic breast cancer. *Clin Cancer Res* **23**, 4190–4202.

[30] Blanco E and Ferrari M (2014). Emerging nanotherapeutic strategies in breast cancer. *Breast* **23**, 10–18.

[31] Ferrari M (2010). Frontiers in cancer nanomedicine: directing mass transport through biological barriers. *Trends Biotechnol* **28**, 181–188.

[32] Nizzero S, Ziemys A, and Ferrari M (2018). Transport barriers and oncophysics in cancer treatment. *Trends Cancer* **4**, 277–280.

[33] Michor F, Liphardt J, Ferrari M, and Widom J (2011). What does physics have to do with cancer? *Nat Rev Cancer* **11**, 657–670.

[34] Mpekris F, Angeli S, Pirentis AP, and Stylianopoulos T (2015). Stress-mediated progression of solid tumors: effect of mechanical stress on tissue oxygenation, cancer cell proliferation, and drug delivery. *Biomech Model Mechanobiol* **14**, 1391–1402.

[35] Munson JM and Shieh AC (2014). Interstitial fluid flow in cancer: implications for disease progression and treatment. *Cancer Manag Res* **6**, 317–328.

[36] Ziemys A, Yokoi K, and Kojic M (2015). Capillary collagen as the physical transport barrier in drug delivery to tumor microenvironment. *Tissue Barriers* **3**e1037418.

[37] Yokoi K, Kojic M, Milosevic M, Tanei T, Ferrari M, and Ziemys A (2014). Capillary-wall collagen as a biophysical marker of nanotherapeutic permeability into the tumor microenvironment. *Cancer Res* **74**, 4239–4246.

[38] Laginha KM, Verwoert S, Charrois GJ, and Allen TM (2005). Determination of doxorubicin levels in whole tumor and tumor nuclei in murine breast cancer tumors. *Clin Cancer Res* **11**, 6944–6949.

[39] Aceto N, Toner M, Maheswaran S, and Haber DA (2015). En route to metastasis: circulating tumor cell clusters and epithelial-to-mesenchymal transition. *Trends Cancer* **1**, 44–52.

[40] Aceto N, Bardia A, Miyamoto DT, Donaldson MC, Wittner BS, Spencer JA, Yu M, Pely A, Engstrom A, and Zhu H, et al (2014). Circulating tumor cell clusters are oligoclonal precursors of breast cancer metastasis. *Cell* **158**, 1110–1122.

[41] Gomez-Cuadrado L, Tracey N, Ma R, Qian B, and Brunton VG (2017). Mouse models of metastasis: progress and prospects. *Dis Model Mech* **10**, 1061–1074.

[42] Fidler IJ (2003). The pathogenesis of cancer metastasis: the 'seed and soil' hypothesis revisited. *Nat Rev Cancer* **3**, 453–458.

[43] Bugyik E, Renyi-Vamos F, Szabo V, Dezso K, Ecker N, Rokusz A, Nagy P, Dome B, and Paku S (2016). Mechanisms of vascularization in murine models of primary and metastatic tumor growth. *Chin J Cancer* **35**, 19.

[44] Paez-Ribes M, Man S, Xu P, and Kerbel RS (2016). Development of patient derived xenograft models of overt spontaneous breast cancer metastasis: a cautionary note. *PLoS One* **11**e0158034.